SAND2019-15374C

AN UNBALANCED SINUOUS ANTENNA FOR ULTRA-WIDEBAND POLARIMETRIC GROUND-PENETRATING RADAR

*Dylan A. Crocker**

Sandia National Laboratories
ISR EM & Sensor Technologies
Albuquerque, New Mexico, USA

Waymond R. Scott, Jr.

Georgia Institute of Technology
School of Electrical and Computer Engineering
Atlanta, Georgia, USA

ABSTRACT

Sinuous antennas are capable of producing ultra-wideband radiation with polarization diversity in a low-profile form factor, making them a good fit for close-in sensing applications such as ground-penetrating radar (GPR). In this work, each arm of a four-port sinuous antenna is operated independently to achieve a quasi-monostatic antenna system capable of polarimetry while separating transmit and receive channels, as is common in GPR systems. The quasi-monostatic configuration of the antenna reduces system size as well as increasing sensitivity to near-surface targets by preventing extreme bistatic angles. A prototype four-port sinuous antenna is fabricated and integrated into a GPR testbed. The polarimetric data obtained with the antenna is then used to distinguish between buried target symmetries.

***Index Terms*—** Antennas, broadband antennas, ground-penetrating radar, radar antennas, sinuous antennas.

1. INTRODUCTION

The ability of ground-penetrating radars (GPRs) to reliably detect and classify subterranean targets is often hampered by large amounts of non-interest targets or "clutter." In order to correctly discriminate between desired targets and clutter, target information must be accurately inferred from the received signals. Target shape information may be obtained by analyzing the polarization of the scattered wave relative to the polarization of the transmitted wave. This technique is referred to as polarimetry and has significant application in the classification of targets [1, 2]. However, most currently fielded GPR systems utilize singularly polarized antennas to reduce system size and complexity. Furthermore, GPR antennas are usually operated bistatically to simplify the electronics and the antenna feeds. However, a bistatic configuration may result in extreme off-boresight angles when attempting to detect near-surface targets, e.g., landmines, as illustrated in Fig. 1. At such angles, the transmit and receive radiation patterns may not well overlap, resulting in reduced sensitivity. Additionally, at off-boresight angles, antennas often have reduced polarization purity and pattern uniformity over the operating band. Therefore, a polarimetric GPR antenna, operated in either a monostatic or quasi-monostatic configuration, is desired.

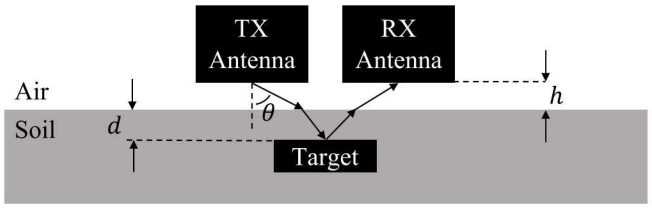

Fig. 1: Diagram of GPR scenario with bistatic antenna configuration resulting in undesirable extreme bistatic angles when $d + h$ is small, i.e., near-surface targets.

Sinuous antennas are capable of producing polarization-diverse radiation with relatively constant gain over ultra-wide bandwidths in a low-profile form factor [3]. Other wideband antenna designs provide similar capabilities; however, they require relatively large and often complex three-dimensional structures in order to produce orthogonal senses of polarization [4]. Furthermore, the sinuous antenna was recently shown to be capable of transmitting and receiving temporally short pulses for GPR applications [5, 6]. In this work, a sinuous antenna is proposed for near-surface GPR applications with a novel feeding arrangement. More specifically, each arm of the sinuous antenna is operated independently [7], thereby allowing the separation of transmit and receive channels while still providing dual-polarized radiation in a quasi-monostatic configuration, i.e., small bistatic angles. A prototype antenna is developed and experimentally integrated into a GPR testbed, where it is used to provide polarimetric data capable of discriminating between target symmetries.

*This work was supported in part by Sandia National Laboratories, a multimission laboratory managed and operated by National Technology and Engineering Solutions of Sandia, LLC., a wholly owned subsidiary of Honeywell International, Inc., for the U.S. Department of Energy's National Nuclear Security Administration under contract DE-NA0003525. This paper describes objective technical results and analysis. Any subjective views or opinions that might be expressed in the paper do not necessarily represent the views of the U.S. Department of Energy or the United States Government.

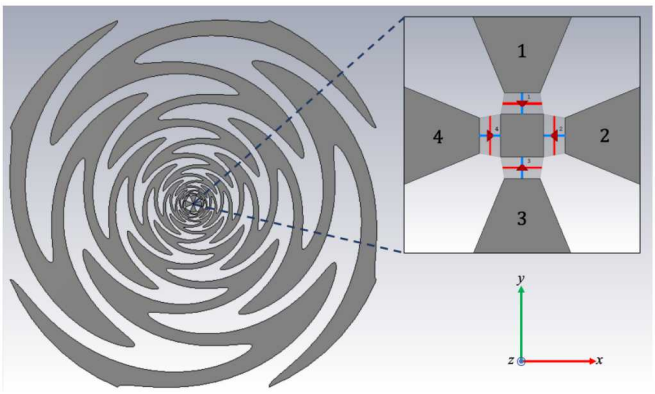

Fig. 2: Model of unbalanced four-arm sinuous antenna. The antenna pictured is based on the improved design developed in [5] and has parameters: $N = 4$ arms, $P = 12$ cells, $R_T = 9.5$ cm, $\tau = 0.773$, $\alpha = 45°$, and $\delta = 22.5°$. Each arm is driven independently against a common reference as indicated by the red ports.

Fig. 3: Prototype four-port sinuous antenna with absorber loaded cavity backing. The inset shows a CAD model of the coaxial cable feed with the substrate hidden to visualize the connection to the antenna arms.

2. UNBALANCED SINUOUS ANTENNA

A four-arm sinuous antenna, based on the improved design developed in [5], was investigated with each arm driven independently, as illustrated in Fig. 2. Such a configuration allows for the separation of the transmit and receive channels, which reduces system complexity by precluding the need for baluns and directional couplers. The sinuous antenna geometry is well defined in the literature [3, 5] and will not be repeated here for brevity.

With the configuration shown in Fig. 2, ports 1 and 3 will produce radiation polarized predominately in the $\hat{x}$ direction. On the other hand, ports 2 and 4 will produce radiation polarized predominately in the $\hat{y}$ direction. In this work, ports 1 and 2 will be designated for transmission, while ports 3 and 4 will be used for reception. The corresponding polarization scattering matrix [8] is thus defined as

$$\begin{bmatrix} S_{HH} & S_{HV} \\ S_{VH} & S_{VV} \end{bmatrix} = \begin{bmatrix} S_{31} & \frac{1}{2}(S_{32}+S_{41}) \\ \frac{1}{2}(S_{32}+S_{41}) & S_{42} \end{bmatrix}, \quad (1)$$

where the cross-polarized terms are have been averaged to produce a more symmetric response, i.e., $S_{HV} = S_{VH}$. Circular polarization (CP) can then be achieved by driving two orthogonal ports, e.g., ports 1 and 2, with a $\pm 90°$ phase progression. However, this complicates the feeding structure by requiring a hybrid-coupler. Alternatively, circular polarization may be synthesized, given $j = \sqrt{-1}$, as [8]

$$\begin{bmatrix} S_{LL} & S_{LR} \\ S_{RL} & S_{RR} \end{bmatrix} = \frac{1}{2}\begin{bmatrix} 1 & -j \\ 1 & +j \end{bmatrix}\begin{bmatrix} S_{HH} & S_{HV} \\ S_{VH} & S_{VV} \end{bmatrix}\begin{bmatrix} 1 & 1 \\ -j & +j \end{bmatrix}. \quad (2)$$

Exciting only a single arm of the antenna will tilt the beam off of boresight; however, in the near-field, the area under the antenna is well illuminated as will be made evident with the experimental results. Furthermore, transmitting and receiving on opposite arms results in symmetric CP sensitivities [9].

A prototype of the proposed four-port sinuous antenna was fabricated for further analysis and is pictured in Fig. 3. The antenna was manufactured using an LPKF PCB milling machine out of 1.575 mm (0.062") thick Rogers RT/duroid® 5880 laminate (1 oz. copper clad). The addition of the substrate lowers the average input impedance to approximately 197 Ω over the 1–10GHz band [9]. A simple direct connection of coaxial cables feeds each arm of the antenna individually, as shown in Fig. 3. This connection is similar to that in [10], but here each cable is operated as an independent channel. The antenna also implements a cavity loaded with AN-79 absorber to absorb the back lobe of the radiation for integration with a GPR testbed. The final antenna height is approximately 14.5 cm. It may be possible to reduce the height of the cavity without sacrificing much performance [9]; however, the cavity and absorber were selected based on availability from another project [11].

3. EXPERIMENTAL GPR INTEGRATION

The GPR testbed consists of a three-axis positioner and vector network analyzer (VNA), both of which are connected to a controlling desktop computer. A sand-filled pit, in which targets may be buried, is located directly under the measurement apparatus. Fig. 4 shows the antenna mounted to the positioner and lowered to approximately 5 cm above the leveled sand. The measurement data is collected with the VNA in the frequency domain as 4-port S-parameters from 10 MHz to 8 GHz in 10 MHz steps. The data is then transformed to the time domain via an IFFT after being weighted with a Taylor window having parameters $\bar{n} = 15$ and $PSR = -80$ as defined in [8]. The time-domain result of a single measurement

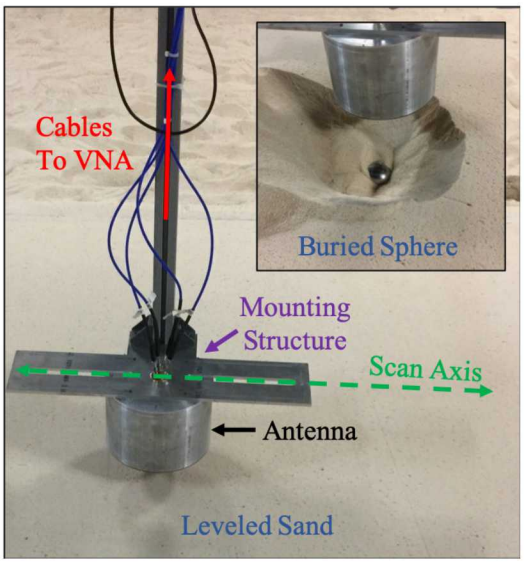

Fig. 4: Experimental GPR Measurement Setup.

is called an A-scan [12]. An ensemble set of A-scans produced by the positioner movement is referred to as a B-scan or a C-scan for 1-D and 2-D positioner scans, respectively [12]. When the positioner is moved, it is allowed to settle mechanically before the VNA records data. This procedure is referred to as the "stop-and-stare" method, which is slower than performing data acquisition during continuous movement but provides increased accuracy.

Two different targets were measured, each buried approximately 5 cm below the surface of the sand. The first target is a 5.08 cm diameter sphere, which represents a symmetric target. The second target is a 10.1 cm wire oriented at 45° to the x-axis, which represents a target with a high degree of asymmetry. The raw measured data is not ideal as it contains mutual coupling between the antenna ports as well as phase drift in the measurement equipment. Coherent background subtraction was used to calibrate the target responses. A measurement sample taken away from the target was used as the background and a phase alignment procedure compensated for any drift. The background subtraction also removed a significant amount of the response from the surface of the sand; however, the smoothed surface is not perfectly level, which leaves a remnant of the surface return in the data. Dispersion in the antenna is compensated by applying a phase correction similar to that developed in [6]. Dual linear data is collected, which is then used to synthesize CP responses using the transform described in (2).

The antenna was scanned over a two-dimensional grid (C-scan) for each of the buried targets; the resulting three-dimensional data are displayed in Fig. 5 and Fig. 6 for the sphere and wire, respectively. The C-scan data consists of multiple x-axis B-scans made at different y-axis locations. The background was subtracted by removing the $x = 40$ cm

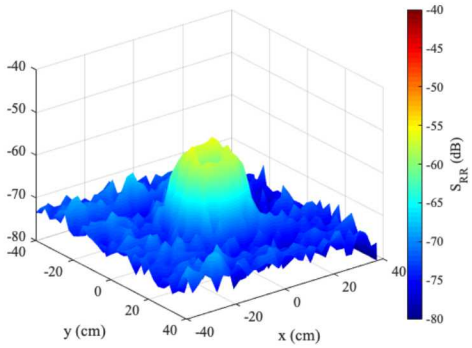

(a) S_{LL}

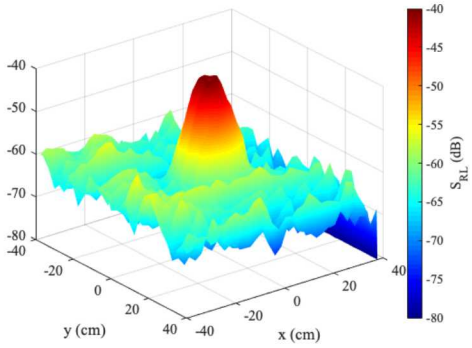

(b) S_{LR}

Fig. 5: C-scan measurement results for the 5.08 cm sphere buried 5 cm in the sand.

sample from each B-scan. Since the C-scan represents a four-dimensional data set, it can be challenging to visualize effectively. For the results shown in Fig. 5, and Fig. 6, the peak response in time was taken for each (x,y) sample. The peak search began after 2.2 ns in order to avoid the primary response from the surface. The peak-search is not a particularly useful method for processing real-world data—especially when the scene contains multiple targets; although, the technique was adequate for the simple case analyzed.

The returns from symmetric targets (e.g., spheres) may be distinguished from those from asymmetric targets (e.g., wires) by comparing the co- and cross-polarized components [4]. Symmetric targets will primarily produce a co-polarized CP response, while asymmetric targets will produce both co- and cross-polarized CP responses. False-color maps were created from the CP responses, similar to those developed in [113], which allow for visual discrimination between symmetric and asymmetric targets. The false-color maps are created from the measured B-scan data by setting all pixels 12 dB below the peak response of the target to white while setting the red, green, and blue components of the remaining pixels to

$$\begin{bmatrix} R \\ G \\ B \end{bmatrix} = \begin{bmatrix} \frac{|S_{RL}|}{|S_{LL}|} \\ 0 \\ \frac{|S_{RL}|-|S_{LL}|}{|S_{RL|}} \end{bmatrix}. \tag{3}$$

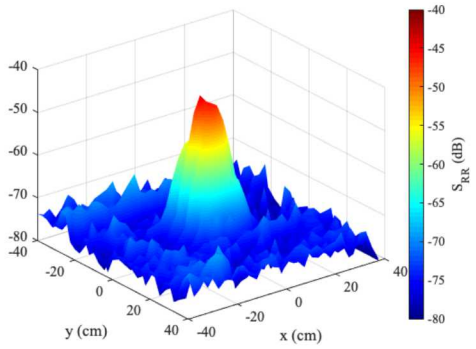

(a) S_{LL}

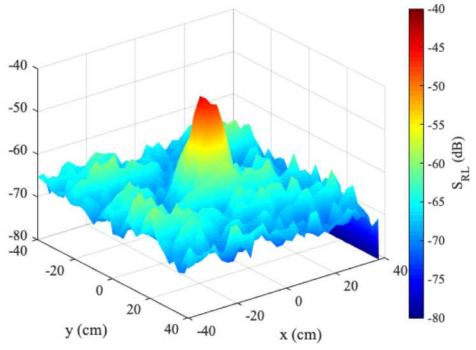

(b) S_{LR}

Fig. 6: C-scan measurement results for the 10.1 cm wire buried 5 cm in the sand.

With this color mapping, symmetric targets will appear blue, and asymmetrical targets will appear red in the image.

The CP data presented in Fig. 5 and Fig. 6 were then used to create the false-color maps shown in Fig. 7 using (3). As can be observed, the CP responses were successfully used to discriminate between symmetric and asymmetric targets by comparing the ratio of co- and cross-polarized returns.

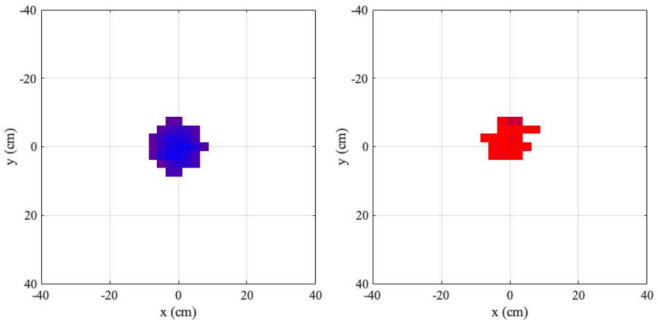

(a) 5.08 cm Sphere (b) 10.1 cm Wire

Fig. 7: False color map generated for the buried sphere (left) and wire (right) targets.

4. REFERENCES

[1] V. Kabourek, P. Černý, and M. Mazánek, "Landmine detection using ground penetrating radar and polarimetric synthetic aperture radar," in *Proceedings of the 5th European Conference on Antennas and Propagation (EUCAP)*, 4 2011, pp. 34–38.

[2] Y. Yu, C. Chen, X. Feng, and C. Liu, "Application of entropy classification method to the detection of subsurface linnear targets in polarimetric GPR data," in *Geoscience and Remote Sensing Symposium (IGARSS), 2016 IEEE International*. IEEE, 2016, pp. 7438–7441.

[3] R. H. DuHamel, "Dual polarized sinuous antennas," U.S. Patent US4658262A, Apr. 14, 1987.

[4] J. Sustman, *Analysis of resistive-vee dipole antennas for producing polarization diversity*, Ph.D. thesis, School of Electrical and Computer Engineering, Georgia Institute of Technology, 6 2014.

[5] D. A. Crocker and W. R. Scott, "On the design of sinuous antennas for uwb radar applications," *IEEE Antennas and Wireless Propagation Letters*, vol. 18, no. 7, pp. 1347–1351, 7 2019.

[6] D. A. Crocker and W. R. Scott, "Compensation of dispersion in sinuous antennas for polarimetric ground penetrating radar applications," *Remote Sensing*, vol. 11, no. 15, 2019.

[7] H. Emami, N. Sarkhosh, E. Lara, and A. Mitchell, "Reconfigurable photonic feed for sinuous antenna," *Journal of Lightwave Technology*, vol. 30, no. 16, pp. 2725–2732, 8 2012.

[8] M. A. Richards, J. A. Sheer, and W. A. Holm, Eds., *Principles of Modern Radar*, vol. 1 of *3*, SciTech, Edison, NJ, 7 2010.

[9] D. A. Crocker, *Numerical and Experimental Evaluation of Sinuous Antennas for Remote Sensing Applications*, Ph.D. thesis, School of Electrical and Computer Engineering, Georgia Institute of Technology, Dec. 2019.

[10] Y. Kang and K. Kim, "Experimental validation of removal of sharp ends in sinuous antenna arms," in *2013 Asia-Pacific Microwave Conference Proceedings (APMC)*, 11 2013, pp. 212–214.

[11] M. McFadden, *Analysis of the equiangular spiral antenn*, Ph.D. thesis, School of Electrical and Computer Engineering, Georgia Institute of Technology, 11 2009.

[12] D. J. Daniels, Ed., *Ground Penetrating Radar*, Electromagnetics and Radar Series. Institution of Engineering and Technology, 2nd edition, 2004.